Physics of Plasmas

RESEARCH ARTICLE | JANUARY 02 2025

Experimental and computational evaluation of alpha particle production from laser-driven proton–boron nuclear reaction in hole-boring scheme

M. Huault ; T. Carrière; H. Larreur ; Ph. Nicolaï ; D. Raffestin ; D. Singappuli ; E. D'Humieres ; D. Dubresson ; K. Batani ; M. Cipriani ; F. Filippi ; M. Scisciò; C. Verona ; L. Giuffrida ; V. Kantarelou ; S. Stancek ; N. Boudjema ; R. Lera ; J. A. Pérez-Hernández ; L. Volpe; M. D. Rodríguez Frías ; A. Bonasera; M. R. D. Rodrigues; D. Ramirez Chavez; F. Consoli ; D. Batani

Phys. Plasmas 32, 013102 (2025)
https://doi.org/10.1063/5.0238029

Experimental and computational evaluation of alpha particle production from laser-driven proton–boron nuclear reaction in hole-boring scheme

Cite as: Phys. Plasmas **32**, 013102 (2025); doi: 10.1063/5.0238029
Submitted: 9 September 2024 · Accepted: 12 November 2024 ·
Published Online: 2 January 2025

View Online Export Citation CrossMark

M. Huault,[1,a)] T. Carrière,[2] H. Larreur,[1,2] Ph. Nicolaï,[2] D. Raffestin,[2] D. Singappuli,[2] E. D'Humieres,[2] D. Dubresson,[2] K. Batani,[3] M. Cipriani,[4] F. Filippi,[4] M. Scisciò,[4] C. Verona,[5] L. Giuffrida,[6] V. Kantarelou,[6] S. Stancek,[6,7] N. Boudjema,[8,9] R. Lera,[9] J. A. Pérez-Hernández,[9] L. Volpe,[9,10] M. D. Rodríguez Frías,[9,11] A. Bonasera,[12,13] M. R. D. Rodrigues,[13] D. Ramirez Chavez,[13] F. Consoli,[4] and D. Batani[2]

AFFILIATIONS

[1]Departamento de Física Fundamental, Universidad de Salamanca, 37008 Salamanca, Spain
[2]Université de Bordeaux, CNRS, CEA, CELIA, Unité Mixte de Recherche 5107, Talence 33400, France
[3]IPPLM Institute of Plasma Physics and Laser Microfusion, Hery Street 23, 01-497 Warsaw, Poland
[4]ENEA Nuclear Department-C. R. Frascati, Via Enrico Fermi 45, 00044 Frascati, Italy
[5]Dipartimento di Ingegneria Industriale, Università di Roma "Tor Vergata," Via del Politecnico 1, 00133 Roma, Italy
[6]ELI Beamlines Facility, The Extreme Light Infrastructure ERIC, 252 41 Dolni Brezany, Czech Republic
[7]Joint Laboratory of Optics of Palacky University and IOP of Academy of Sciences of the Czech Republic, 779 00 Olomouc, Czech Republic
[8]Departamento de Física Aplicada, Universidad de Salamanca, 37008 Salamanca, Spain
[9]Centro de Láseres Pulsados, Edificio M5, Parque Científico, 37185 Salamanca, Spain
[10]ETSIAE Universidad Politécnica de Madrid, 28006 Madrid, Spain
[11]Departamento de Física y Matemáticas, Universidad de Alcalá, 28871 Madrid, Spain
[12]Laboratori Nazionali del Sud, Istituto Nazionale di Fisica Nucleare (LNS-INFN), 95123 Catania, Italy
[13]Cyclotron Institute, Texas A&M University, College Station, Texas 77843, USA

[a)]**Author to whom correspondence should be addressed:** marine.huault@outlook.fr

ABSTRACT

The majority of studies on laser-driven proton–boron nuclear reaction is based on the measurement of α-particles with solid-state nuclear tracks detector (Cr39). However, Cr39's interpretation is difficult due to the presence of several other accelerated particles which can bias the analysis. Furthermore, in some laser irradiation geometries, cross-checking measurements are almost impossible. In this case, numerical simulations can play a very important role in supporting the experimental analysis. In our work, we exploited different laser irradiation schemes (pitcher–catcher and direct irradiation) during the same experimental campaign, and we performed numerical analysis, allowing to obtain conclusive results on laser-driven proton–boron reactions. A direct comparison of the two laser irradiation schemes, using the same laser parameters is presented.

I. INTRODUCTION

Presently, high-brightness α-particle sources are obtained in dedicated cyclotrons, such as ARRONAX[1] or U-120M,[2] which accelerate He-nuclei to energies higher than 10 MeV. Such machines generally produce a few 10 μA of α-particles on target, corresponding to about 10^{14} α/s. One of the main applications of bright α-particles sources is in the medical domain, i.e., the production of radioisotopes important either for diagnostics (PET imaging[3]) or medical treatment (vectorized

radiotherapy[4]). Both approaches can also be merged together into theranostics[5] leading to more personalized medical treatments. However, the short lifetime of many radioisotopes limits the use of radiopharmaceuticals only to the medical centers located near the cyclotron.

Several recent experiments with laser-produced plasma based on proton–boron nuclear reaction ^{11}B(p, α)2 α showed unexpectedly high α-particle yields, thus offering the possibility of developing sources based on a radically new technology, i.e., laser-driven high brightness α-particles sources. Indeed, this new approach could allow to realize more compact, cheaper, and handier sources which could find place in many more medical centers, virtually reducing to zero the distance between the production and the use of the radioisotopes.

Most experiments used high-intensity lasers to produce a bright source of protons through the mechanism of target normal sheath acceleration (TNSA)[6] from a target called "pitcher." These were directed on a secondary boron target (called "catcher") where the proton–boron reactions took place and α-particles were produced[7] (so-called "pitcher–catcher" configuration). Alternatively, the laser could directly irradiate a boron target (containing hydrogen) where boron and hydrogen nuclei were accelerated by various mechanisms, including radiation pressure acceleration[8] (RPA), to finally react producing 3 α-particles[9] (so-called "direct irradiation scheme").

In the pitcher–catcher geometry, intermediate measurements, like the space phase of protons before interaction with boron, can be done and facilitate the analysis of nuclear reactions. Furthermore, the separation between the pitcher and the catcher allows a cleaner detection of α-particles safe from laser–matter interaction region, which is an intense source of particles and radiations. In the direct irradiation geometry, none of the previous simplifications apply. In addition, the main diagnostic to measure α-particles is based on solid-state nuclear track detectors like Cr39. Unfortunately, these detectors are also sensitive to protons and ions, which are present in a large number and may bias α-particle detection. A possible way to explore the direct irradiation geometry is to use a large set of simulations with dedicated numerical tools but in any case, reliable experimental data are required to constrain and give confidence in computations.

We report here the results from an experimental campaign realized with the high repetition rate short pulse VEGA-3 PW laser system at the CLPU facility, exploiting the two laser irradiation schemes, pitcher–catcher and direct irradiation. In both geometries, the laser intensity, pulse duration, and focal spot diameter are identical. The first part of the campaign in the pitcher–catcher configuration is reproduced and analyzed using particle in cell (PIC) simulations,[10] providing a validation of the numerical tools and the laser/target parameters used in the simulation. The second part dedicated to the direct irradiation is interpreted using the same numerical tools allowing to obtain conclusive results.

II. THE EXPERIMENTAL CAMPAIGN CONDITIONS

A. Laser parameters

The experiment was performed with the Ti:Sa laser system VEGA-3 at the CLPU facility, which may deliver 30 J in a pulse duration of 30 fs corresponding to a laser power of 1 PW at a wavelength of 800 nm. The laser spot diameter, at full width at half maximum, is about 11 μm but only 25 % of the energy is inside the central peak. During the experiment, the laser-interaction with target was optimized to get the most stable proton spectrum, the pulse duration was then adjusted to 200 fs, and intensity on target was $\approx 3.5 \times 10^{19}$ W/cm^2. The contrast was about 2×10^{-5} at 1 ps before the main pulse and below 10^{-5} at 5 ps.

B. Diagnostics

During the campaign, both geometries, pitcher–catcher, and direct irradiation have been tested, using the same diagnostics. Under the conditions of laser–matter interaction, several ions species are accelerated at the front and at the rear sides of the target, mainly originating from the contaminant layer. Hence, the low rate of ^{11}B(p, α)2 α nuclear reaction makes the discrimination between α-particles and other accelerated ion species difficult. To estimate the number of α-particles emitted from boron target, we used several diagnostics with complementary detection methods, either for direct measurements such as (i) Thomson parabola spectrometer,[11] (ii) solid state nuclear track detector,[12] or indirect via (iii) high purity germanium detector.[13] Each diagnostic presents some drawbacks, but the combination may help to infer the correct amount of nuclear reactions taking place.

1. Thomson parabola (TP)

TP diagnostic allows deflecting ion species with different mass-over-charge (m/q) ratios on different parabolic trajectories. Our TP had magnetic field of 0.8 T (horizontal deflection) and electric field of few kV/cm (vertical deflection). A 200 μm diameter pinhole was used at the entrance of the TP, and a calibrated Image plate MS type was used for the detection.[14] However, ions having the same charge to mass ratio are on the same parabola trace and cannot be discriminated.

2. Solid state nuclear track detector (Cr39)

Cr39 gives a direct information about charged particle fluency. After irradiation, the plastic polymer is etched in a caustic solution (5.6 M NaOH at 70° for an hour) to reveal tracks produced by ions interaction with the polymer. Each ion producing a track, this diagnostic may allow single particle detection. Nevertheless, two different ions having different energies may produce the same track.[15] To solve this issue, a thin layer of aluminum may be set in front of the CR39. Indeed, the range of a particle depends on its energy and charge, and a given filter thickness may help discriminating between different ions. In this experiment, the Cr39 have a thickness of 1.5 mm and area of 2×2 cm^2 separated into four equal regions covered by different aluminum filters (thickness of 5, 10, and 15 μm), where one region had no filter (see Fig. 1). Cr39 have been calibrated with α-particles from the accelerator AIFIRA[16] and Pu^{239} source up to 5 MeV (LP2I, Gradignan).

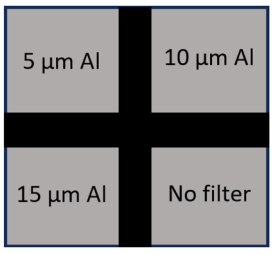

FIG. 1. Aluminum filter regions placed on Cr39.

3. High purity germanium detector (HPGe)

HPGe allows tracing back to the number of reactions $^{11}B(p, \alpha)2\,\alpha$ that have occurred in the target by measuring γ-rays emitted from the decay of elements produced in secondary reactions with single photon counting. Indeed, nuclear reactions between proton and boron produce gamma emitter radioisotopes giving a clear signature of the reactions (i.e., ^{7}Be or ^{11}C). Knowing the branching ratio, the measurement of nuclear products can give information on the main investigated reaction. However, this diagnostic is a post-shot measurement, requiring an intact target for the analysis. This may be the case in the pitcher–catcher geometry but not in the direct irradiation, due to the ablation of matter by the laser.

III. PITCHER–CATCHER SCHEME

A. Pitcher–catcher: Setup

Figure 2 shows the setup in pitcher–catcher scheme. TNSA protons produced from the interaction of VEGA-3 with a 6 μm thick aluminum foil (pitcher) of 99 % purity, tilted at 12° with respect to laser axis, interact on a catcher of natural Boron B (80 % ^{11}B, 20% ^{10}B, thickness 2 mm, dimension 2.5 × 2.5 cm^2) or boron-nitride BN (50% ^{14}N, 40% ^{11}B, 10% ^{10}B, thickness 5 mm, dimension 5 × 5 cm^2) to generate α-particles by proton–boron fusion reactions.[17] B catcher was tilted at ≈45° from pitcher normal axis and placed at 24 mm from pitcher. BN catcher was tilted at 70° from pitcher normal axis and placed at 43 mm from pitcher. Positions and compositions of the different catchers are gathered in Table I.

Thick catchers were used to maximize the proton–boron interaction over a longer path. Indeed, higher-energy protons penetrate more deeply and even if the p-B cross section is smaller, they integrate the interaction probability over a longer range and finally also go through the sub-MeV resonance (i.e., 675 keV). Tilts of ≈45° and 70° have been tested to observe the difference in the detection efficiency of alpha-particles.

Table II presents the position of diagnostics with respect to targets used in this scheme. TP was used to characterize the TNSA proton and ions spectrum emitted from aluminum pitcher rear side, when the catcher was not present. The signal was accumulated for tens of successive shots with identical interaction parameters and then averaged.

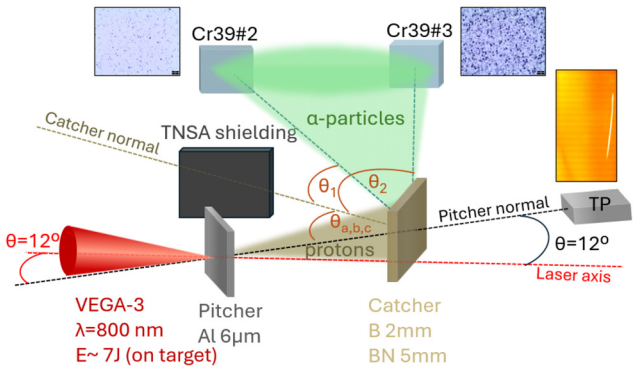

FIG. 2. Experimental setup for the pitcher–catcher scheme. VEGA-3 laser impinges on the 6 μm aluminum target (pitcher). The resulting TNSA protons accelerated at the rear side of the pitcher interact with the B-type catcher target to produce α-particles. Diagnostic positions with respect to targets are mentioned in Table II.

TABLE I. Catcher positions and compositions.

Catcher	Thickness (mm)	Dimensions (mm)	Distance to pitcher (mm)	Tilt[a] (deg)	Density (g/cm^3)
B#1	2	25 × 25	24	$\theta_a = 45$	2.37
B#2	2	25 × 25	24	$\theta_b = 48$	2.37
BN	5	50 × 50	43	$\theta_c = 70$	2.2

[a]Angle of catcher with respect to pitcher normal axis.

Several Cr39 (respectively, called #2 and #3) were placed at different angles with respect to the normal of catcher front side and accumulated the signal during all the shot session, with same laser parameter conditions. A 1 cm thick aluminum shielding protects Cr39 #2 from direct emission of TNSA protons and ions accelerated from pitcher rear side layer, and allows particle detection from catcher emission only.[17] Cr39 #3 was looking at both the catcher front side and pitcher rear side emission. Catcher samples were inserted inside the HPGe detector after each shot session to measure the γ-rays emissions from ^{7}Be and ^{11}C decays.

B. Pitcher–catcher: Experimental results

The pitcher–catcher geometry allows the measurement of the laser driven protons responsible of the nuclear reactions within boron. Figure 3 shows the results from the direct interaction of VEGA-3 with the pitcher target only, where proton spectrum up to 17 MeV has been measured with the TP. Several shot series have shown the stability of the proton beam phase-space. Protons come from the pollutant layer presents at the rear side of the aluminum target. Other ions, present in this layer, are also accelerated, like C^{5+} up to 35 MeV, as shown in Fig. 3.

In total, 50 shots have been realized to test the TNSA shielding efficiency to protect Cr39 #2. Figure 4 shows a pictures of Cr39 #2 and #3 areas in the filtered region of 5 μm Al thickness. As expected, the detector placed at position #2 behind the shielding shows no presence of interaction with particles, while #3 clearly shows many tracks.[17]

In the presence of catcher target, particles have been detected in the three filtered regions of Cr39 #2, behind the shielding. According to simulations (see Sec. III C), most of the particles detected on Cr39 #2 are either pitcher protons deflected by the borated catcher, or protons and α-particles directly produced in the catcher. Thanks to the calibration of Cr39, α-particle spectra have been reconstructed from

TABLE II. Diagnostic positions in the pitcher–catcher scheme.

	Target: Pitcher		Target: Catcher (B and BN)	
Diagnostic	Distance[a] (cm)	Angle[a] (deg)	Distance[a] (cm)	Angle[a] (deg)
TP	62.5	0	...	...
Cr39 # 2	...	...	52(B); 51.7(BN)	$\theta_1 = 55$(B); $\theta_1 = 30$(BN)
Cr39 # 3	58	55	56.7(B); 55.6(BN)	$\theta_2 = 80$(B); $\theta_2 = 55$(BN)

[a]Positions with respect to target normal axis (pitcher or catcher).

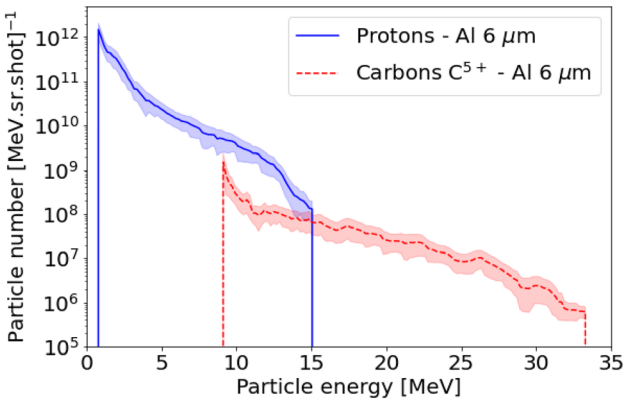

FIG. 3. Experimental spectrum of proton and carbon ions from 6 μm aluminum target rear side, obtained with TP diagnostic. Low energy carbons are cut by the coating layer of the IP model (for MS type, about 8.5 MeV).

the three filtered regions, under the assumption that no alphas with energy lower than about 1 MeV reached the CR39 detector, and that protons tracks were reasonably small.[15] Spectra showed an estimated energy cutoff close to 7 MeV (see Fig. 5).

Figure 6 compares the total α-particle number in each filtered region for B and BN targets. Each catcher had a different tilt with respect to pitcher normal axis. We observe that BN catcher shows the same order of magnitude in α-particle yield of the B catcher even if it contains two times less boron. The reason is indeed related to the tilt at higher angles (70°). At high angle tilt, more proton–boron fusion reactions occur close to the surface of the catcher due to the grazing angle of protons. Hence, in this geometry more α-particles, especially low energy ones which have only a few μm mean free path can escape as they are generated closer to the surface. In addition, we can observe an enhancement of α-yield for 5 μm Al thickness filters in the case of BN catcher. According to simulations (Sec. III C), the catcher tilted at 70° considerably increases the diffusion of carbons. Since it is not possible to distinguish carbon from α, the measurement is overestimated, essentially in the 5 μm aluminum filter region of Cr39.

To summarize, in pitcher-catcher geometry using B catcher, up to 3.3×10^6, 2.9×10^6, and 1.6×10^6 α/sr/shot have been detected in the region of 5, 10, and 15 μm Al filter of the Cr39 # 2, corresponding to α-particles with energy higher than 1.6, 2.8, and 4 MeV, respectively. These numbers should be reduced to take into account the carbon contribution (see Sec. III C). In the case of BN catcher, the same magnitude has been measured, 7.5×10^6, 3.2×10^6, and 9.5×10^5 α/sr/shot,

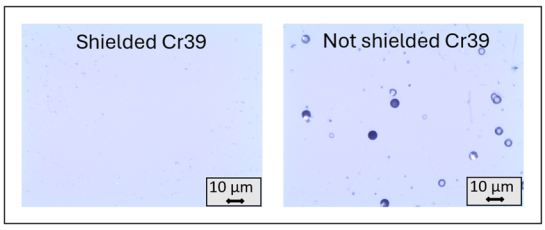

FIG. 4. Detection comparison between Cr39 at position #2 (left), protected by the TNSA shielding and #3 (right) not shielded during laser irradiation on 6 μm Al target.

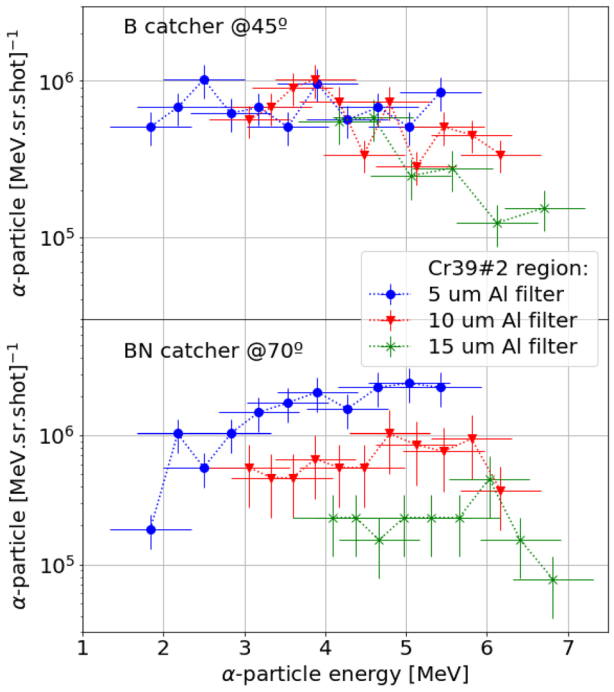

FIG. 5. Experimental α-particle spectra obtained with Cr39 #2 from B (top) and BN (bottom) samples in the pitcher–catcher scheme. Original spectra are reconstructed from different filtered regions of 5, 10, and 15 μm aluminum thicknesses.

respectively, for energies greater than 1.6, 2.8, and 4 MeV. We note that the α number estimated in the 5 μm Al filtered region for BN catcher must be interpreted with caution, since a strong carbon contribution is expected according to simulations (see Sec. III C). We note that an uncertainty of 25.5% (B catcher) and 43.7% (BN catcher), due to the standard deviation of the track counts in the observed filtered regions by optical microscopy, must be taken into account in the interpretation of the experimental results.

In order to get an additional confirmation of our results on α-particle generation from BN catcher, we also used a γ-ray diagnostic. In

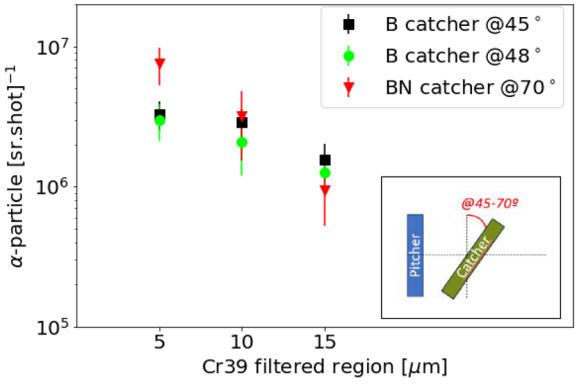

FIG. 6. α-particle estimation for different catchers and angles (from 45° to 70°), in the pitcher–catcher scheme.

this case, after the irradiation, the BN catcher was analyzed using a high purity germanium (HPGe) detector equipped with a DSA-1000, 16 K channel integrated multichannel analyzer and cooled with liquid nitrogen at 77 K. The catcher was placed inside a lead container screening it from external radiation sources for an acquisition time of 13 h and 21 min. The environmental γ-ray background was taken into account and detector was calibrated as shown in Ref. 18. The measured γ-ray spectrum shows the presence of peaks at 511 and 477 keV (see Fig. 7). This first one is coming mainly from ^{11}C produced by the following reaction:

$$p + {}^{11}B \rightarrow {}^{11}C + n - 2.765\,\text{MeV} \quad (1)$$

with a half-lifetime of T= 20.44 min. The peak at 477 keV is due to the ^{7}Be radioisotope decay produced by the reaction

$$p + {}^{10}B \rightarrow {}^{11}C^{*} \rightarrow {}^{7}Be + \alpha$$

with a half-lifetime of T= 53.22 days.

The initial activities reported per shot on the HPGe diagnostic give $A(^{7}Be)$= 0.8 Bq/s and $A(^{11}C)$= 9.5 kBq/s. The number of reactions can be traced back with the following equation:

$$N = \frac{A}{\lambda} \quad (2)$$

with A being the sample activity per second and $\lambda = \ln(2)/T$ being the decay constant (s^{-1}). We finally find

$$N(^{7}Be) = 5.3 \times 10^{6}/\text{shot}$$
$$N(^{11}C) = 1.6 \times 10^{7}/\text{shot}.$$

Further details about the method of analysis can be found in Ref. 18.

C. Pitcher–catcher: Comparison with simulations and discussion

The particle-in-cell (PIC) code Smilei has been used to simulate the laser plasma interaction in 2D geometry. In a second step, the proton phase-space has been injected in the Monte Carlo code FLUKA[19–21] to compute the nuclear reactions. In the experiment, a pre-plasma in front of the interaction zone was present at the time of main laser pulse interaction, due to amplified spontaneous emission (ASE) induced in the laser system. In the PIC simulation, a density gradient length of 0.1 μm is assumed. The density of the aluminum target is fixed at 50 times the critical density. The simulation domain is discretized in a $128 \times 128\,\mu m^2$ grid with a constant mesh size of $30 \times 30\,nm^2$. Each cell with matter contains 80 particles.

Figure 8 presents the comparison between experimental proton spectra from TP diagnostic obtained in distinct days with the simulated one. The good agreement gives confidence in the simulation and validates the choice of assumptions used in the code as well as the laser and target parameters, which allows accessing to non-measured data as the angular distribution of protons used to initialize the MC code.

In the presence of catcher target, several tracks have been detected on the Cr39 #2 placed behind the shielding. At first sight, we expect to detect mostly α, the diameters of the tracks seem to correspond to different ion species. MC simulations (FLUKA) have been done to explore the emission of particles from the catcher target in the direction of the Cr39 detector. The simulated proton spectrum previously obtained was used as an input source, and a detection box was placed at the position of Cr39 #2. According to simulations (see Fig. 9), the main contributions of particles emitted from catcher are α from proton–boron reactions and protons diffused by the catcher or induced by nuclear reactions inside the catcher. These are typically a few 10^{-5} per incident proton. Diffused carbons are also observed in the case of carbon spectrum in input, with a ratio of a few 10^{-6} carbon per incident carbon for a catcher at 45° and a few 10^{-5} for a catcher at 70°. This diffusion is negligible in the Cr39 filtered region of 10 and 15 μm aluminum, which need carbons greater than 11.5 and 17.5 MeV, which are in very low numbers compared to protons, according to our experimental carbon spectrum. However, ≈6 MeV carbon is enough to cross 5 μm Al filter. Considering a similar carbon and proton number at this energy range, the carbon diffusion could influence the estimation of α-particles up to 10 % for the B catcher and a factor 2 for the BN catcher.

Fragmentation products can be discarded, since fragmentation takes place for carbon energy higher than 12 MeV, and therefore, in negligible number with our experimental carbon spectrum (see Fig. 3). The possibility of extracting boron is also ruled out, with a ratio 100 times lower than α-particle emission, considering protons or carbons as input source.

Simulations allow testing effects of two parameters (density and incident angle) on the nuclear reaction rate. A direct comparison

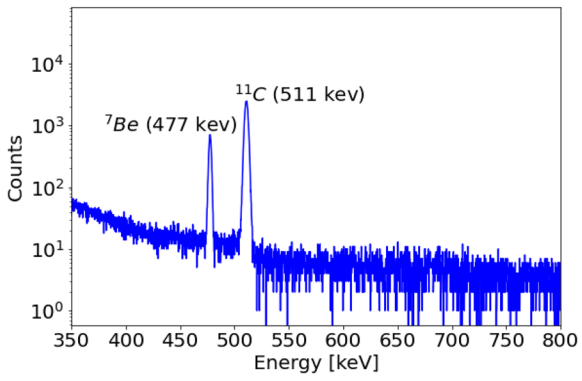

FIG. 7. Measured γ-spectra from BN catcher with the HPGe diagnostic.

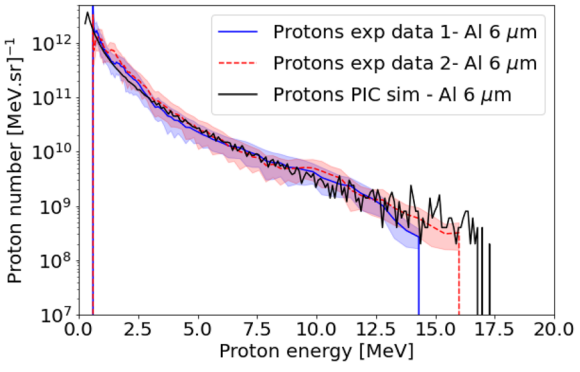

FIG. 8. Comparison of experimental spectra obtained with TP diagnostic in distinct days (data 1 averaged on 20 shots and data 2 averaged on 5 shots) with simulated spectrum obtained with Smilei PIC code.

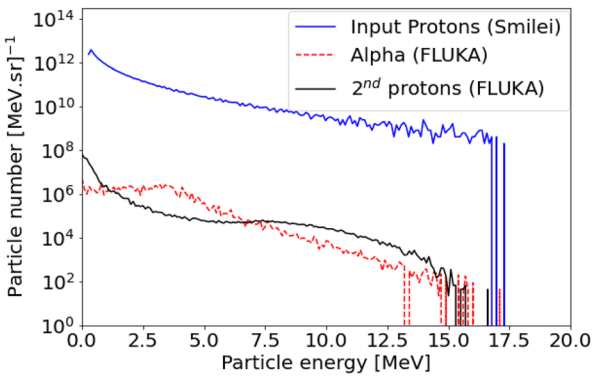

FIG. 9. Simulation in the pitcher–catcher scheme. Output proton and α spectra, emitted from the front side of the boron catcher are represented, as well with the input proton spectrum. The output spectra, respectively, named "second protons (FLUKA)" and "α (FLUKA)," are obtained with FLUKA MC simulation. The input proton spectrum was obtained previously with PIC simulation (Smilei) and inserted in MC simulation. The second protons are obtained from diffusion on the catcher and nuclear reactions inside with the catcher.

between a B catcher at a density of 2.37 g/cc and a BN target at 2.2 g/cc, both irradiated by a proton beam at 45° with respect to the normal, yields, respectively, to 4 and 2×10^7 α-particles. Changing the incident angle to 70° for the BN catcher increases the α-particle number by a factor 1.7 (3.3×10^7 α-particles), close to the number obtained with B catcher at an incident angle of 45° and in agreement with the experimental results. In the last step, the α-particle spectrum has been propagated through 5, 10, and 15 μm Al filter to provide a direct comparison with the Cr39 measurements. From the B target, 6×10^6 α/sr cross 5 μm of aluminum, 4×10^6 α/sr cross 10 μm, and 1×10^6 α/sr, 15 μm whereas from BN catcher, one obtains 5×10^6 α/sr, 3×10^6 α/sr, and 1×10^6 α/sr, respectively (see Table III for summary).

We rely on MC simulations to relate the number of produced ^7Be and ^{11}C, to the number of produced α-particles in the catcher (2.6×10^8 α) and escaping ones (3.3×10^7 α and hence be collected by

TABLE III. Summary of α-particle detection in the pitcher–catcher scheme with the Cr39 #2 detector.

			α-particle number [sr shot]$^{-1}$ in Cr39 #2 region:		
	Catcher	Angle with respect to pitcher normal (deg)	5 μm Al	10 μm Al	15 μm Al
exp	B#1	45	3.0×10^6 [a] (3.3×10^6)	2.9×10^6	1.6×10^6
sim			6×10^6	4×10^6	1×10^6
exp	B#2	48	2.7×10^6 [a] (3.0×10^6)	2.1×10^6	1.3×10^6
sim			6×10^6	4×10^6	1×10^6
exp	BN	70	3.8×10^6 [a] (7.5×10^6)	3.2×10^6	9.5×10^5
sim			5×10^6	3×10^6	1×10^6

[a]Value corrected with carbon contribution.

TABLE IV. Estimation of the branching ratio between ^{7}Be and ^{11}C and α-particles in the BN catcher with MC simulations. α^{out} are the total α emitted from the catcher and α^{in} are the total α produced inside the catcher.

A B	^{7}Be	^{11}C	α^{in}
α^{out}	Ratio A/B = 3.3	Ratio A/B = 1.7	Ratio A/B = 0.12

CR39 # 2 detector). Simulation results show that in the case of BN, with the typical dimension of our catcher and using the simulated proton spectrum shown in Fig. 8, only ≈12 % of generated α-particles can escape from the catcher front side (and zero from rear side). They also show that the ratio between the number of escaping α with respect to the number of produced ^7Be and ^{11}C is 3.3 and 1.7, respectively (see Table IV). MC simulations give $\approx 1 \times 10^7$ produced ^7Be and $\approx 2 \times 10^7$ produced ^{11}C. Hence, these calculations are again in good agreement with data obtained experimentally with the HPGe, by a factor number of ≈1.9 for ^7Be and ≈1.3 for ^{11}C.

IV. DIRECT IRRADIATION SCHEME

A. Direct irradiation: Setup

Table V shows the positions of diagnostics used in this scheme. In this configuration (see Fig. 10), the VEGA-3 laser interacts directly with a 100 μm thick boron-nitride target (50% ^{14}N, 40% ^{11}B, and 10% ^{10}B) coated by 2 μm plastic layer (CH) on the front and rear side (we will call the target CH-BN-CH in the following) placed at 30° with respect to laser axis, with a density of 2.2 ± 0.1 g/cm^3. In this configuration scheme, a 100 μm target thickness was considered to be thick enough to stop all RPA protons (few MeV). 2 μm plastic is enough to avoid the direct laser interaction with BN material. In previous experiments, the quantity of hydrogen in the target was unknown and, therefore, did not allow us to go back to reliable simulation results. Thus, adding a coated plastic of known proportion made it possible to insert the right proportions of hydrogen in PIC simulation and to obtain proton spectrum closer to the experimental one. The proton phase-space after the plastic layer is extracted from PIC simulation and then inserted in FLUKA simulation to interact with the BN target and produce nuclear reactions.

TP diagnostic was placed at the target rear side accumulating TNSA ions emission for tens of shots. α-particle emission from CH-BN-CH target front side was characterized using two Cr39 (#5 and #6) exposed during the entire shot session at two different angles in the target equatorial plane.

TABLE V. Diagnostic positions in direct irradiation scheme.

	Reference: target CH-BN-CH	
Diagnostic	Distance[a] (cm)	Angle[a] (deg)
TP	62.5	18 (rear)
Cr39 # 5	36	26 (front)
Cr39 # 6	27	38 (front)

[a]Positions with respect to target normal axis (front and rear side).

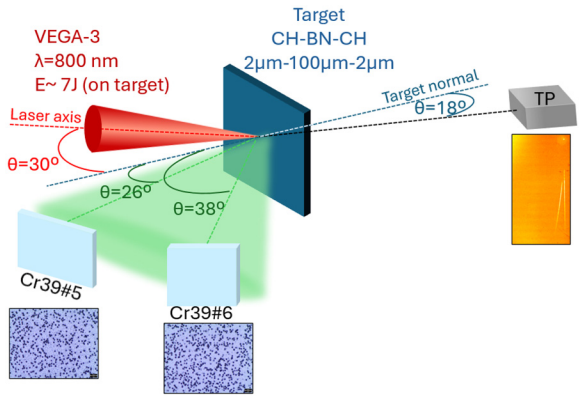

FIG. 10. Experimental setup for the direct irradiation scheme. VEGA-3 laser interacts directly with the CH-BN-CH target. Production of α-particle occurs inside the target between RPA protons and Boron ions. Positions with respect to target are mentioned in Table V.

B. Direct irradiation: Experimental results

In this configuration, diagnostics are exposed to all particles accelerated from the CH-BN-CH target at the front and rear sides and no shielding is possible. 10 shots on TP placed at target rear side show the presence of a proton population with energy cutoff close to 3.5 MeV (see Fig. 11). Neither the presence of α-particle nor carbon ion has been observed on TP. Note that the IP type MS has a coating blocking α-particles with energy lower than 3 MeV and carbon lower than 8.5 MeV.

Cr39 placed at front side are exposed to all particles accelerated by TNSA. In order to distinguish α-particle contribution from heavier ions, the detectors were placed at different angles with respect to the target normal axis to test the emission anisotropy. Apart from protons, the laser interaction with the 2 μm CH coated layer accelerates carbon ions. To try discriminating between Carbons and α-particles, 10 and 15 μm aluminum filters were placed in front of the Cr39. These thicknesses, respectively, stop 11.5 and 17.5 MeV carbons, meaning that the α-particle count will be correct only if carbon ions have lower energies. Figure 12 shows the particle distribution at 26° and 38° from target normal. For a given filter thickness, the amount of detected particles is similar and in agreement with an isotropic distribution. Cr39 #5 detects α-yield around 1.6×10^6 and 3.9×10^5 α/sr/shot in the region of 10 and 15 μm thick aluminum filter, corresponding to energies greater than 2.8 and 4 MeV, respectively. Cr39 #6 detects α-yield around 2.1×10^6 and 2.4×10^5 α/sr/shot in the region of 10 and 15 μm thick aluminum filter. Thinner filtered regions were saturated. We note that an uncertainty of 38.5%, due to the standard deviation of the track counts in the observed filtered regions by optical microscopy, must be taken into account in the interpretation of the experimental results.

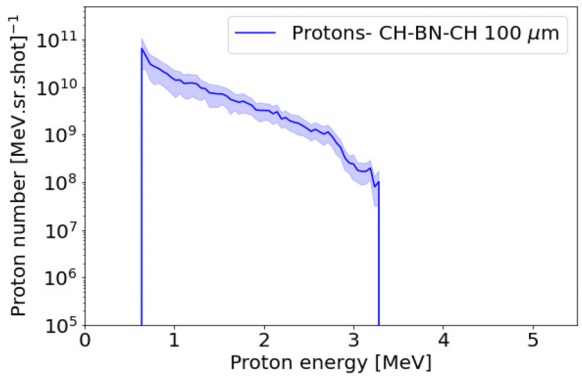

FIG. 11. Experimental proton spectrum from 100 μm BN target rear side (both faces coated with 2 μm CH), obtained with TP diagnostic.

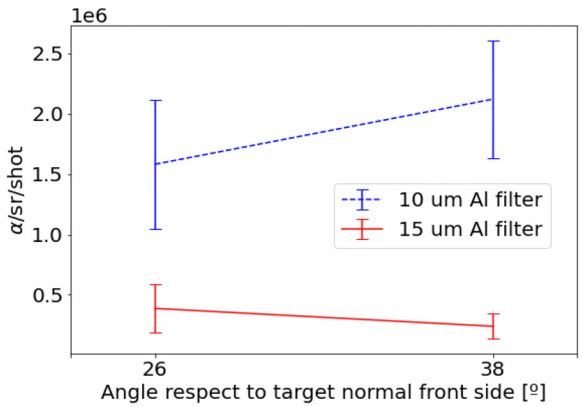

FIG. 12. Angular distribution of α-particle detected on Cr39 #5 and #6 for regions filtered with aluminum thicknesses of 10 and 15 μm in the direct irradiation scheme.

Figure 13 represents the experimental α spectrum reconstructed from Cr39 #5 and #6 in the region of 10 and 15 μm aluminum filters, using our calibration. Once again, it seems that regardless the position of Cr39 at 26° or 38°, the spectral distribution of the α-particle is similar, strengthening the isotropic emission hypothesis.

C. Direct irradiation: Comparison with simulations and discussion

Contrary to the pitcher–catcher geometry, the laser driven protons, triggering nuclear reactions cannot be directly measured.

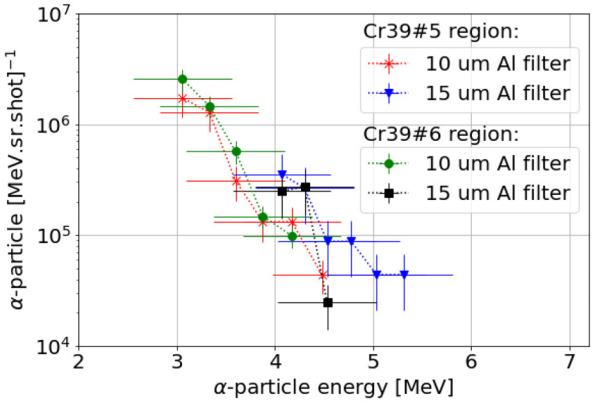

FIG. 13. Experimental α-particle spectra obtained with Cr39 #5 and #6 in the direct irradiation scheme. Original spectra are reconstructed from different regions of 10 and 15 μm aluminum thicknesses.

However, some measurements like the proton emission at the rear side of the target thanks to the TP can reinforce the confidence in simulation results. Figure 14 shows the energy-angular distributions of protons, carbons, and α-particles computed by the PIC and MC codes (for PIC, the density of the aluminum target is fixed at 50 times the critical density. The simulation domain is discretized in a $256 \times 128\,\mu m^2$ grid with a constant mesh size of $30 \times 30\,nm^2$. Each cell with matter contains 80 particles). The difference in emission is clearly distinguishable. Particles resulting from the laser driven acceleration have a peaked angular distribution, with an energy decreasing sharply with the angle with respect to the target normal, while particles from a nuclear reaction are rather isotropic. At the rear side, TNSA protons present a maximum energy of 3.5 MeV in agreement with the TP measurements.

Although multi-MeV protons are present at the rear side, no α-particles are detectable. This means that protons accelerated by RPA process are not energetic enough to cross 100 μm of BN and produce nuclear reactions at the rear side (i.e., α-particles). Hence, the multi-MeV protons present at the rear side are those produced by TNSA from the target surface rear side. Carbon ions are also accelerated at the rear side but due to the MS imaging plate used, they cannot be detected.

Cr39 placed at the front side of the target detected all particles emitted from the front side of the catcher, in particular, carbon ions which could be confused with α-particles. The main difference between them concerns the angular distribution. Simulation results indicate that even a small change in direction should strongly modify the measurement for carbons but not for α-particles. In addition, except close to the target normal, where carbon energies can reach 30 MeV, at 26° and 38° with respect to the target normal, their energies are too small to cross the aluminum filters of 10 and 15 μm Al and so cannot be measured in CR39. It is worth noting that carbon has been used for simulation since it is the ion with the lowest stopping power among the components of the contaminant layer (appart from hydrogen) and present in the CH deposited layer. Finally, in these conditions, only α-particles and protons are detected by the CR39. Simulation estimate the α-particle number to 4×10^5 α/sr and 1×10^5 α/sr after 10 and 15 μm, respectively (see Table VI for summary).

V. CONCLUSIONS

This work presents experimental results on α-particle production in p-B reactions initiated by the PW laser VEGA-3 in two configuration schemes. The study of the pitcher–catcher scheme and its comparison with numerical simulations helped to validate our code and give confidence in the simulation tool and the parameters to be used for simulating the direct irradiation scheme. The α-particles were estimated experimentally with solid state nuclear track detectors Cr39. The use of filters in front of Cr39 allowed to discriminate the contribution of protons and heavy ions from α-particles, and, thanks to the calibration performed with the AIFIRA accelerator and a radioactive source, we were able to reconstruct the α-particle spectra.

In the pitcher–catcher scheme, $\approx 2.9 \times 10^6$ and 3.2×10^6 α/sr/shot have been estimated for energies higher than 2.8 MeV, with a cut-off around 7 MeV, respectively, for the B and BN catchers. The comparison with the simulations helped to quantify and characterize the particles emitted from the catcher reaching the Cr39 detectors. The main contribution of detected particle on Cr39 in the 10 and 15 μm Al filtered region comes from proton and α-particles in similar number

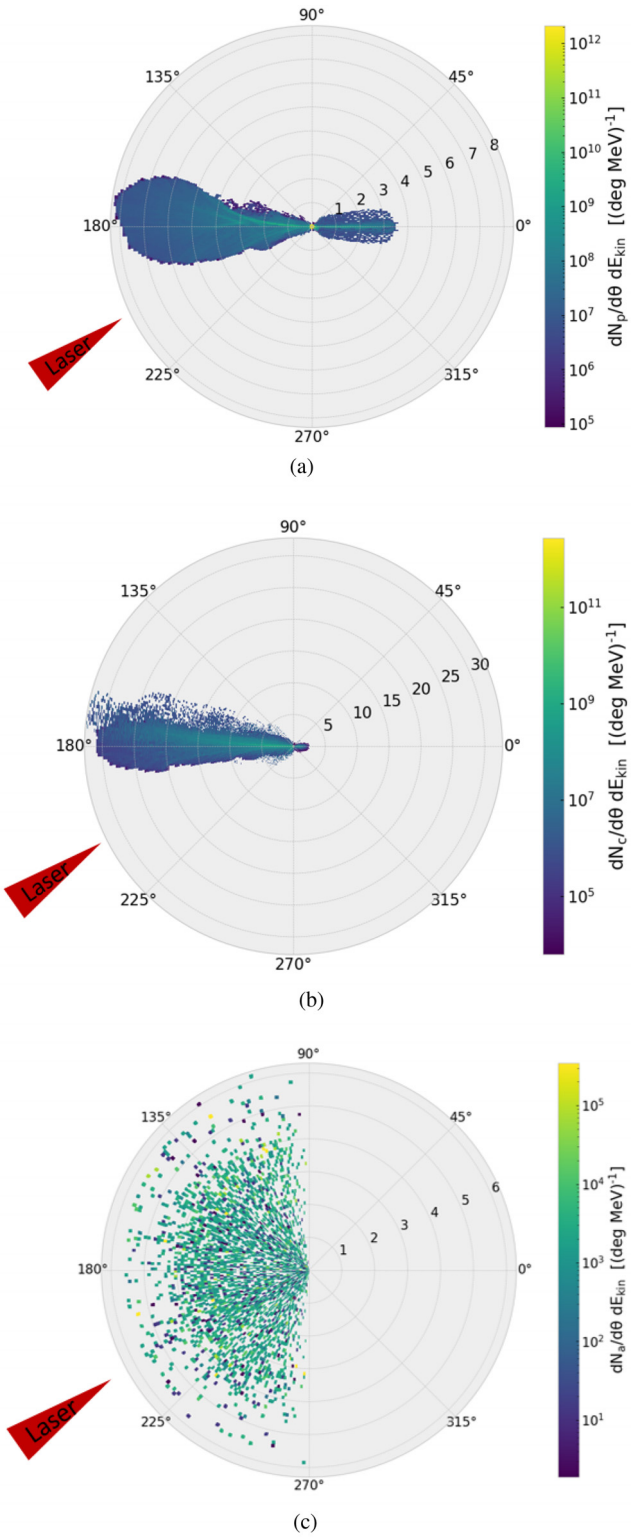

FIG. 14. Angular distribution of proton (a), carbons (b), and α-particles (c). Laser impinges from left side. Circular slices represent the particle energy.

TABLE VI. Experimental and numerical comparison of α-particle detection in direct-irradiation scheme with Cr39 #5 and #6 detectors.

	Target	Angle of target with respect to laser axis (deg)	α-particle number [sr shot]$^{-1}$ in Cr39 region: 10 μm Al	15 μm Al
			Cr39#5	
exp	CH-BN-CH	30	1.6×10^6	3.9×10^5
sim	CH-BN-CH	30	4×10^5	1×10^5
			Cr39 #6	
exp	CH-BN-CH	30	2.1×10^6	2.4×10^5
sim	CH-BN-CH	30	4×10^5	1×10^5

(a few 10^{-5}/incident proton). One should interpret numbers with caution in the 5 μm filtered region of Cr39 (i.e., $\alpha > 1.6$ MeV) since carbon diffusion can increase the α estimation by 10% for B catcher and a factor 2 for BN catcher. We observe that tilting the catcher target to a higher angle with respect to pitcher normal axis may favor the production of α-particle in layers close to the surface of the catcher, from where they can more easily escape, thus enhancing their detection.

In the direct irradiation scheme, comparison between experimental data and simulations allowed us to infer the number of α-particles, despite a direct exposure of Cr39 to TNSA pollutants. Thanks to the positioning of the detectors and the use of filters, we were able to distinguish the different contributions from α-particles and heavier ions. α-particles close to 6 MeV have been detected, and we estimated their number to a 2.1×10^6 α/sr/shot for energies higher that 2.8 MeV. Finally, it is interesting to compare our results with other recent results reported in scientific literature. Figure 15 shows the comparison. Obviously, due to the lower laser energy available on the VEGA-3 facility, as compared to KJ laser installations like LFEX and PALS, the number of α-particles obtained is lower than in previous experiments.

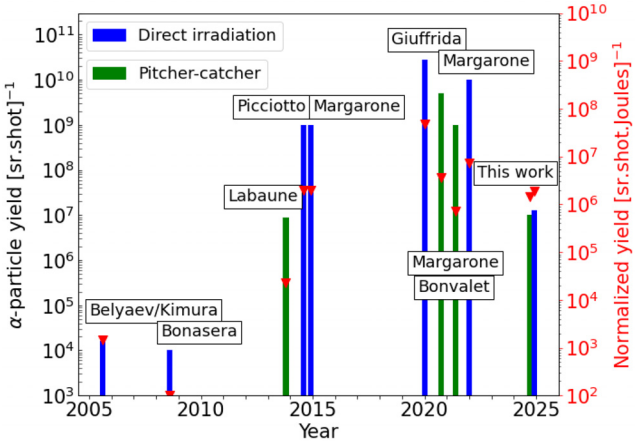

FIG. 15. Experimental progresses in the two configuration schemes in term of α-particle production in "direct irradiation"[9,22–27] and "pitcher–catcher" geometries.[7,28,29]

However, in our case, only α-particles above 1.6 MeV are counted. The total number of α-particles that should be emitted experimentally on the front side target before filters can be retrieved thanks to simulation and is up to $\approx 1 \times 10^7$ α/sr/shot in the pitcher–catcher, and 1.3×10^7 α/sr/shot in direct irradiation. When comparing the results displayed in this graph normalized to the laser energy, the α-yield per unit of energy is similar. Thus, it might, indeed, be advantageous to use high repetition rate for developing α-particle sources. If we have $\approx 1 \times 10^7$ α/shot/sr with 7 J on the target, we need about ≥ 1000 shots to reach similar α-yield obtained with big KJ-class lasers such as LFEX.[9] Working at 1 Hz, this will require an accumulation time of ≈15 min which is still much shorter than the typical repetition rate of big lasers. At 10 Hz, which is currently feasible, the accumulation time will be further reduced.

ACKNOWLEDGMENTS

This work has been supported by COST (European Cooperation in Science and Technology) through the Action CA21128 PROBONO (PROton BOron Nuclear Fusion: from energy production to medical applicatiOns). It also has received funding from the European Union's 2020 research and innovation programme under the Grant Agreement No. 101008126, corresponding to the RADNEXT project. We acknowledge the support of HB11 Energy Holdings Pty, Australia, through its Collaborative Science Program. This work was granted access to the HPC resources of TGCC under the Allocation Nos. 2023-A0140514117 made by GENCI. We acknowledge the financial support of the IdEx University of Bordeaux/Grand Research Program "GPR LIGHT," and of the Graduate Program on Light Sciences and Technologies of the University of Bordeaux. This work was supported in part by the United States Department of Energy under Grant No. DEFG02-93ER40773. We acknowledge to the Unidad de Investigación Consolidada de la Junta de Castilla y Leon UIC-167. Finally, we thank the Laser, Radioprotection, Engineering, TIC areas, and Management divisions of the CLPU for their valuable support.

AUTHOR DECLARATIONS

Conflict of Interest

The authors have no conflicts to disclose.

Author Contributions

M. Huault: Formal analysis (equal); Investigation (equal); Supervision (equal); Writing – original draft (equal). **T. Carrière:** Formal analysis (equal). **H. Larreur:** Investigation (equal). **Ph. Nicolaï:** Investigation (equal); Supervision (equal); Validation (equal); Writing – review & editing (equal). **D. Raffestin:** Investigation (equal); Supervision (equal); Validation (equal); Writing – review & editing (equal). **D. Singappuli:** Investigation (equal). **E. D'Humières:** Investigation (equal). **D. Dubresson:** Formal analysis (equal). **K. Batani:** Investigation (equal). **M. Cipriani:** Investigation (equal). **F. Filippi:** Investigation (equal). **M. Scisciò:** Investigation (equal). **C. Verona:** Investigation (equal). **L. Giuffrida:** Investigation (equal). **V. Kantarelou:** Investigation (equal). **S. Stanček:** Investigation (equal). **N. Boudjema:** Investigation (equal). **R. Lera:** Investigation (equal).

J. A. Pérez Hernández: Investigation (equal). **L. Volpe:** Investigation (equal). **M. D. Rodríguez Frías:** Investigation (equal). **A. Bonasera:** Investigation (equal). **M. R. D. Rodrigues:** Investigation (equal). **D. Ramirez Chavez:** Investigation (equal). **F. Consoli:** Investigation (equal). **D. Batani:** Investigation (equal); Supervision (equal); Validation (equal); Writing – review & editing (equal).

DATA AVAILABILITY

The data that support the findings of this study are available from the corresponding author upon reasonable request.

REFERENCES

[1]F. Haddad, L. Ferrer, G. Arnaud, T. Carlier, N. Michel, J. Barbet, and J.-F. Chatal, "ARRONAX, a high-energy and high-intensity cyclotron for nuclear medicine," Eur. J. Nucl. Med. Mol. Imaging **35**, 1377–1387 (2008).

[2]See https://www.ujf.cas.cz/en/departments/department-of-accelerators/cyclotron/ for information about the Cyclotron U-120M.

[3]K. W. D. Ledingham, P. McKenna, T. McCanny, S. Shimizu, J. M. Yang, L. Robson, J. Zweit, J. M. Gillies, J. Bailey, G. N. Chimon, R. J. Clarke, D. Neely, P. A. Norreys, J. L. Collier, R. P. Singhal, M. S. Wei, S. P. D. Mangles, P. Nilson, K. Krushelnick, and M. Zepf, "High power laser production of short-lived isotopes for positron emission tomography," J. Phys. D **37**, 2341 (2004).

[4]N. Lepareur, B. Ramée, M. Mougin-Degraef, and M. Bourgeois, "Clinical advances and perspectives in targeted radionuclide therapy," Pharmaceutics **15**(6), 1733 (2023).

[5]C. L. Wright, J. Zhang, M. F. Tweedle, M. V. Knopp, and N. C. Hall, "Theranostic imaging of yttrium-90," BioMed. Res. Int. **2015**, 481279.

[6]A. Macchi, M. Borghesi, and M. Passoni, "Ion acceleration by superintense laser-plasma interaction," Rev. Mod. Phys. **85**, 751–793 (2013).

[7]J. Bonvalet, P. Nicolaï, D. Raffestin, E. D'humieres, D. Batani, V. Tikhonchuk, V. Kantarelou, L. Giuffrida, M. Tosca, G. Korn, A. Picciotto, A. Morace, Y. Abe, Y. Arikawa, S. Fujioka, Y. Fukuda, Y. Kuramitsu, H. Habara, and D. Margarone, "Energetic α-particle sources produced through proton-boron reactions by high-energy high-intensity laser beams," Phys. Rev. E **103**, 053202 (2021).

[8]A. Macchi, F. Cattani, T. V. Liseykina, and F. Cornolti, "Laser acceleration of ion bunches at the front surface of overdense plasmas," Phys. Rev. Lett. **94**, 165003 (2005).

[9]D. Margarone, J. Bonvalet, L. Giuffrida, A. Morace, V. Kantarelou, M. Tosca, D. Raffestin, P. Nicolaï, A. Picciotto, Y. Abe, Y. Arikawa, S. Fujioka, Y. Fukuda, Y. Kuramitsu, H. Habara, and D. Batani, "In-target proton–boron nuclear fusion using a PW-class laser," Appl. Sci. **12**, 1444 (2022).

[10]J. Derouillat, A. Beck, F. Pérez, T. Vinci, M. Chiaramello, A. Grassi, M. Flé, G. Bouchard, I. Plotnikov, N. Aunai, J. Dargent, C. Riconda, and M. Grech, "SMILEI: A collaborative, open-source, multi-purpose particle-in-cell code for plasma simulation," Comput. Phys. Commun. **222**, 351–373 (2018).

[11]J. J. Thomson, "Rays of positive electricity," Proc. R. Soc. London A **89**, 1–20 (1913).

[12]R. K. Bull and S. A. Durrani, *Solid State Nuclear Track Detection: Principles, Methods, and Applications*, 1st ed. (Pergamon Press, Oxford, NY, 1987).

[13]M. R. D. Rodrigues, A. Bonasera, M. Scisciò, J. A. Pérez-Hernández, M. Ehret, F. Filippi, P. L. Andreoli, M. Huault, H. Larreur, D. Singappuli, D. Molloy, D. Raffestin, M. Alonzo, G. G. Rapisarda, D. Lattuada, G. L. Guardo, C. Verona, F. Consoli, G. Petringa, A. McNamee, M. La Cognata, S. Palmerini, T. Carriere, M. Cipriani, G. Di Giorgio, G. Cristofari, R. De Angelis, G. A. P. Cirrone, D. Margarone, L. Giuffrida, D. Batani, P. Nicolai, K. Batani, R. Lera, L. Volpe, D. Giulietti, S. Agarwal, M. Krupka, S. Singh, and F. Consoli, "Radioisotope production using lasers: From basic science to applications," Matter Radiat. Extremes **9**, 037203 (2024).

[14]G. Boutoux, D. Batani, F. Burgy, J.-E. Ducret, P. Forestier-Colleoni, S. Hulin, N. Rabhi, A. Duval, L. Lecherbourg, C. Reverdin, K. Jakubowska, C. I. Szabo, S. Bastiani-Ceccotti, F. Consoli, A. Curcio, R. De Angelis, F. Ingenito, J. Baggio, and D. Raffestin, "Validation of modelled imaging plates sensitivity to 1–100 keV x-rays and spatial resolution characterisation for diagnostics for the "PETawatt Aquitaine Laser"," Rev. Sci. Instrum. **87**, 043108 (2016).

[15]C. Baccou, V. Yahia, S. Depierreux, C. Neuville, C. Goyon, F. Consoli, R. De Angelis, J. Ducret, G. Boutoux, J. Rafelski, and C. Labaune, "CR-39 track detector calibration for H, He, and C ions from 0.1–0.5 MeV up to 5 MeV for laser-induced nuclear fusion product identification," Rev. Sci. Instrum. **86**, 083307 (2015).

[16]See https://www.lp2ib.in2p3.fr/aifira/ for information about AIFIRA accelerator.

[17]M. Scisciò, G. Petringa, Z. Zhu, M. R. D. Rodrigues, M. Alonzo, P. L. Andreoli, F. Filippi, F. Consoli, M. Huault, D. Raffestin, D. Molloy, H. Larreur, D. Singappuli, T. Carriere, C. Verona, P. Nicolai, A. McNamee, M. Ehret, E. Filippov, R. Lera, J. A. Pérez-Hernández, S. Agarwal, M. Krupka, S. Singh, V. Istokskaia, D. Lattuada, M. L. Cognata, G. L. Guardo, S. Palmerini, G. Rapisarda, K. Batani, M. Cipriani, G. Cristofari, E. D. Ferdinando, G. D. Giorgio, R. D. Angelis, D. Giulietti, J. Xu, L. Volpe, M. D. Rodríguez-Frías, L. Giuffrida, D. Margarone, D. Batani, G. A. P. Cirrone, A. Bonasera, and F. Consoli, "Laser initiated p-11B fusion reactions in petawatt high-repetition-rates laser facilities," Matter Radiat. Extremes (submitted) (2024); arXiv:2411.04577 (2024).

[18]K. Batani, M. Rodrigues, A. Bonasera, M. Cipriani, F. Consoli, F. Filippi, M. Sciscío, L. Giuffrida, V. Kantarelou, S. Stancek, R. Lera, J. Pérez-Hernández, L. Volpe, E. Turcu, M. Huault, H. Larreur, T. Carrière, P. Nicolaï, D. Raffestin, D. Singappuli, and D. Batani, "Generation of radioisotopes for medical applications using short-pulse, high-intensity lasers," High Power Laser Sci. Eng. (submitted) (2024).

[19]C. Ahdida, D. Bozzato, D. Calzolari, F. Cerutti, N. Charitonidis, A. Cimmino, A. Coronetti, G. L. D'Alessandro, A. Donadon Servelle, L. S. Esposito, R. Froeschl, R. García Alía, A. Gerbershagen, S. Gilardoni, D. Horváth, G. Hugo, A. Infantino, V. Kouskoura, A. Lechner, B. Lefebvre, G. Lerner, M. Magistris, A. Manousos, G. Moryc, F. Ogallar Ruiz, F. Pozzi, D. Prelipcean, S. Roesler, R. Rossi, M. Sabaté Gilarte, F. Salvat Pujol, P. Schoofs, V. Stránský, C. Theis, A. Tsinganis, R. Versaci, V. Vlachoudis, A. Waets, and M. Widorski, "New capabilities of the FLUKA multi-purpose code," Front. Phys. **9**, 788253 (2022).

[20]G. Battistoni, T. Boehlen, F. Cerutti, P. W. Chin, L. S. Esposito, A. Fassò, A. Ferrari, A. Lechner, A. Empl, A. Mairani, A. Mereghetti, P. G. Ortega, J. Ranft, S. Roesler, P. R. Sala, V. Vlachoudis, and G. Smirnov, "Overview of the FLUKA code," Ann. Nucl. Energy **82**, 10–18 (2015).

[21]See https://fluka.cern for information about FLUKA code.

[22]A. Picciotto, D. Margarone, A. Velyhan, P. Bellutti, J. Krasa, A. Szydlowsky, G. Bertuccio, Y. Shi, A. Mangione, J. Prokupek, A. Malinowska, E. Krousky, J. Ullschmied, L. Laska, M. Kucharik, and G. Korn, "Boron-proton nuclear-fusion enhancement induced in boron-doped silicon targets by low-contrast pulsed laser," Phys. Rev. X **4**, 031030 (2014).

[23]D. Margarone, A. Picciotto, A. Velyhan, J. Krasa, M. Kucharik, A. Mangione, A. Szydlowsky, A. Malinowska, G. Bertuccio, Y. Shi, M. Crivellari, J. Ullschmied, P. Bellutti, and G. Korn, "Advanced scheme for high-yield laser driven nuclear reactions," Plasma Phys. Controlled Fusion **57**, 014030 (2015).

[24]L. Giuffrida, F. Belloni, D. Margarone, G. Petringa, G. Milluzzo, V. Scuderi, A. Velyhan, M. Rosinski, A. Picciotto, M. Kucharik, J. Dostal, R. Dudzak, J. Krasa, V. Istokskaia, R. Catalano, S. Tudisco, C. Verona, K. Jungwirth, P. Bellutti, G. Korn, and G. A. P. Cirrone, "High-current stream of energetic α particles from laser-driven proton-boron fusion," Phys. Rev. E **101**, 013204 (2020).

[25]V. S. Belyaev, A. P. Matafonov, V. I. Vinogradov, V. P. Krainov, V. S. Lisitsa, A. S. Roussetski, G. N. Ignatyev, and V. P. Andrianov, "Observation of neutronless fusion reactions in picosecond laser plasmas," Phys. Rev. E **72**, 026406 (2005).

[26]S. Kimura, A. Anzalone, and A. Bonasera, "Comment on "Observation of neutronless fusion reactions in picosecond laser plasmas"," Phys. Rev. E **79**, 038401 (2009).

[27]A. Bonasera, A. Caruso, C. Strangio, M. Aglione, A. Anzalone, S. Kimura, D. Leanza, A. Spitaleri, G. Immè, D. Morelli, and J. Sura, "Measuring the astrophysical S-factor in plasmas," in *Fission and Properties of Neutron-Rich Nuclei* (World Scientific Publishing, 2008), pp. 503–507.

[28]D. Margarone, A. Morace, J. Bonvalet, Y. Abe, V. Kantarelou, D. Raffestin, L. Giuffrida, P. Nicolai, M. Tosca, A. Picciotto, G. Petringa, G. A. P. Cirrone, Y. Fukuda, Y. Kuramitsu, H. Habara, Y. Arikawa, S. Fujioka, E. D'Humieres, G. Korn, and D. Batani, "Generation of α-particle beams with a multi-kJ, Peta-Watt class laser system," Front. Phys. **8**, 343 (2020).

[29]C. Labaune, C. Baccou, S. Depierreux, C. Goyon, G. Loisel, V. Yahia, and J. Rafelski, "Fusion reactions initiated by laser-accelerated particle beams in a laser-produced plasma," Nat. Commun. **4**, 2506 (2013).